https://doi.org/10.5194/egusphere-2025-5831
Preprint. Discussion started: 28 November 2025

Quasi-Lagrangian observations of cloud transitions during the initial phase of marine cold air outbreaks in the Arctic – Part 1: Temporal and spatial evolution

Anna Weber[1], Benjamin Kirbus[2,3], Manfred Wendisch[2], and Bernhard Mayer[1]

[1]Meteorologisches Institut, Ludwig-Maximilians-Universität München, Munich, Germany
[2]Leipziger Institut für Meteorologie (LIM), Universität Leipzig, Leipzig, Germany
[3]Fraunhofer-Institut für Energiewirtschaft und Energiesystemtechnik IEE, Kassel, Germany

Correspondence: Anna Weber (Weber.Ann@physik.uni-muenchen.de)

Abstract. This work aims to quantify the macrophysical and microphysical properties of Arctic mixed-phase clouds and their temporal and spatial evolution during marine cold air outbreaks in the Arctic. In particular, cloud thermodynamic phase partitioning and phase transitions are discussed. To this end, high-resolution observations from the airborne hyperspectral and polarized imaging system specMACS during the HALO–$(\mathcal{AC})^3$ campaign are analyzed within a quasi-Lagrangian framework based on backward trajectories. Six flights targeting marine cold air outbreaks are compared to investigate the variability of cloud evolution and its dependence on the cold air outbreak intensity. With increasing time the airmass spent above open ocean, rising cloud top heights, increasing horizontal cloud extents, and growing effective radii of liquid cloud droplets are reported for all cases. In addition, a phase transition from the liquid water to the mixed-phase regime is detected and the ice fraction increases with time. The variability between the observed cloud properties during the cold air outbreaks is large. Larger and faster increasing cloud top heights and effective radii of liquid cloud droplets are observed during stronger events. In addition, the phase transition from the liquid water to the mixed phase occurs earlier and higher ice fractions are reached during the more intense events. The presented data and analyses provide unique observational data, which can be used to improve the representation of low-level Arctic mixed-phase clouds and their evolution during marine cold air outbreaks in models in the future.

1 Introduction

During marine cold air outbreaks (MCAOs) in the Arctic, cold and dry airmasses are advected over the cold sea ice towards warm open ocean (Papritz and Spengler, 2017; Fletcher et al., 2016). The temperature difference between the cold advected airmasses and the ocean surface can be up to 30 K (Papritz and Spengler, 2017). These large temperature gradients create large surface energy fluxes (sensible and latent heat), intense turbulence, and large heat and moisture fluxes, which may contribute to about 60 % to 80 % of oceanic heat loss during winter in the Nordic Seas and may affect deep water formation and sea ice evolution (Papritz and Spengler, 2017; Svingen et al., 2023). In addition, the strong horizontal temperature gradients between the sea ice surface and ocean skin temperatures lead to convection and the formation of low-level clouds (Papritz and Spengler,

https://doi.org/10.5194/egusphere-2025-5831
Preprint. Discussion started: 28 November 2025

2017). The clouds typically organize into cloud streets oriented along the mean wind direction, and transition into cellular structures further downstream due to a decoupling of the atmospheric boundary layer (ABL) and accompanying precipitation formation (Brümmer, 1999; Gryschka and Raasch, 2005; McCoy et al., 2017; Abel et al., 2017; Pithan et al., 2018; Tornow et al., 2021). With increasing time and distance from the formation location of the MCAO, the ABL typically deepens from a few hundred meters to approximately 1 km to 2 km (Brümmer, 1996). MCAOs are most frequently occurring in winter, but also evolve in spring and autumn (Fletcher et al., 2016). They may be related to severe weather events reaching into the mid-latitudes, including extremely cold periods and heavy snowfall, and to polar lows (Pithan et al., 2018). The Fram Strait is one of the main pathways of MCAOs in the Arctic and intense MCAOs are frequently observed in this region (Papritz and Spengler, 2017; Dahlke et al., 2022). Large-scale as well as high-resolution models are struggling to correctly represent the airmass transformations during meridional transports into and out of the Arctic (Sato et al., 2016; Pithan et al., 2016; Tomassini et al., 2017; Field et al., 2017; Wendisch et al., 2021). Especially the microphysical evolution of clouds during MCAOs is difficult to model (Pithan et al., 2014; McCoy et al., 2015; Tan and Storelvmo, 2019; Field et al., 2014; Abel et al., 2017). Consequently, future projections of Arctic climate properties are uncertain (Smith et al., 2019; Cohen et al., 2020; Block et al., 2020).

The clouds formed during MCAOs are typically of a mixed-phase type and have a typical vertical structure. A geometrically thin layer containing supercooled liquid water is located at the cloud top from which ice crystals form via heterogeneous nucleation and sediment downwards (Morrison et al., 2012). The cloud thermodynamic phase partitioning and its spatial distribution are important quantities since they affect the radiative effect of the clouds (Choi et al., 2014; Matus and L'Ecuyer, 2017). The spatial distribution of supercooled liquid water and ice influences, e.g., the efficiency of the Wegener-Bergeron-Findeisen process, which can lead to rapid glaciation of the clouds (Korolev et al., 2017; Korolev and Milbrandt, 2022), and thus affects the cloud cover and cloud lifetime (Pithan et al., 2014). Climate and general circulation models struggle to correctly represent mixed-phase clouds and their microphysical properties (Morrison et al., 2012; Pithan et al., 2014; Komurcu et al., 2014; Cesana et al., 2015, 2022). In particular, the cloud thermodynamic phase partitioning and the vertical distribution of cloud liquid water are challenging for models of different scales (Inoue et al., 2021; Kretzschmar et al., 2019, 2020).

MCAOs and the related clouds have been studied extensively using reanalysis data, ground-based and ship-borne sampling, airborne in situ and remote sensing measurements, satellite observations, as well as model data. Most studies used an Eulerian perspective with a locally fixed coordinate system, while some others applied a quasi-Lagrangian approach. In the Lagrangian perspective, the coordinate system follows the observed airmass, which allows for investigating its temporal evolution. However, real Lagrangian observations are challenging (Wendisch et al., 2023). Instead, the evolution of airmasses can be studied in a quasi-Lagrangian way by applying backward trajectories (Wendisch et al., 2023, 2025). Several studies focused on the properties of clouds during MCAOs. These include dedicated ground-based and ship-based field campaigns providing Eulerian observations of cloud properties (Uttal et al., 2002; Geerts et al., 2022; Shupe et al., 2022; Lackner et al., 2023; Mages et al., 2023; Xia and McFarquhar, 2024). In addition, the microphysical properties of the different cloud regimes during MCAOs and transitions between them were studied during airborne field campaigns using in situ data (Young et al., 2016; Abel et al., 2017; Lloyd et al., 2018; Michaelis et al., 2022) as well as remote sensing observations (Ruiz-Donoso et al., 2020). Besides, model data were applied to investigate the evolution of clouds in MCAOs (Tornow et al., 2021). Quasi-Lagrangian analyses of cloud

https://doi.org/10.5194/egusphere-2025-5831
Preprint. Discussion started: 28 November 2025

properties during MCAOs combining satellite observations with backward trajectories were carried out by Murray-Watson et al. (2023), Wu and Ovchinnikov (2022), Tornow et al. (2023), Mateling et al. (2023), and Seppala et al. (2025). These studies investigated the temporal evolution of macrophysical and microphysical cloud properties, as derived from MODIS or CloudSat data, and their dependency on the MCAO strength or aerosol conditions. However, satellite observations of Arctic cloud properties are only possible with polar-orbiting satellites and strongly affected by small-scale variability, which is not resolved by the coarse resolution satellite measurements (Ahn et al., 2018; Marchant et al., 2020). The retrieval of cloud thermodynamic phase partitioning and further cloud microphysical properties is especially challenging, and most satellite-based studies are restricted to liquid water clouds. Typical scales of inhomogeneities in Arctic clouds are on the order of a few hundred meters (Schäfer et al., 2017, 2018). These scales can be resolved by high-spatial resolution airborne measurements. Airborne quasi-Lagrangian observations of MCAO clouds in the Arctic were performed during the HALO–$(\mathcal{AC})^3$ campaign (Wendisch et al., 2024). Even though several airborne research campaigns were conducted in the Arctic during the last decades (Forsberg et al., 2023) and some quasi-Lagrangian airborne measurements were collected outside the Arctic (Boettcher et al., 2021), HALO–$(\mathcal{AC})^3$ appears to be the first airborne campaign using a quasi-Lagrangian sampling strategy in the Arctic. Schirmacher et al. (2024) analyzed the evolution of precipitation and other cloud properties in the roll convection regime using radar data in two case studies of a stronger and a weaker MCAO during HALO–$(\mathcal{AC})^3$. However, the evolution of cloud thermodynamic phase and microphysical cloud properties has not been studied in a quasi-Lagrangian approach using high-resolution airborne measurements so far.

This work is based on measurements of the specMACS instrument (Ewald et al., 2016; Weber et al., 2024) during the airborne HALO–$(\mathcal{AC})^3$ field campaign (Wendisch et al., 2024; Ehrlich et al., 2025). HALO–$(\mathcal{AC})^3$ was conducted in March and April 2022. The German High Altitude and LOng range research aircraft (HALO, Krautstrunk and Giez, 2012; Stevens et al., 2019) was based in Kiruna and two further research aircraft (Polar 5 and Polar 6) operated out of Svalbard. The campaign generally aimed at improving the understanding of airmass transformations during meridional transports into and out of the Arctic (Wendisch et al., 2024; Ehrlich et al., 2025). HALO followed a quasi-Lagrangian flight strategy, allowing for studying the evolution of cloud properties during MCAOs. specMACS is a hyperspectral and polarized imaging system operated in a downward-looking perspective on board HALO. It provides high-spatial resolution information about cloud macrophysical and microphysical properties, including quantitative information about cloud thermodynamic phase partitioning.

The objective of this work is to study the temporal and spatial evolution of macrophysical and microphysical properties of clouds during MCAOs in a quasi-Lagrangian way, with a special focus on cloud thermodynamic phase partitioning and phase transitions. For this purpose, measurements of cloud properties from specMACS are combined with backward trajectories. The applied data and methods are introduced in Sect. 2. During HALO–$(\mathcal{AC})^3$ in total six MCAOs were sampled. The cloud evolution is investigated for a strong MCAO in Sect. 3.1. Afterwards, the analyses are extended to all observed cases. The variabiliy between the different observed MCAOs and the dependence of the cloud evolution on the MCAO intensity are discussed in Sect. 3.2. Finally, the results are summarized in Sect. 4. The aim of this work is to provide high spatial and temporal resolution information about the evolution of clouds during the initial phase of MCAOs, which can be used for model evaluation to improve the representation of mixed-phase clouds and airmass transformation during MCAOs. Furthermore, the

https://doi.org/10.5194/egusphere-2025-5831
Preprint. Discussion started: 28 November 2025

data can help to further our understanding of Arctic mixed-phase cloud processes and, in particular, phase changes in these clouds. The analyses of the temporal and spatial cloud evolution during MCAOs presented here are extended to the vertical dimension in the second part of this work in Weber et al. (2025a), which investigates the vertical cloud structure and its evolution based on specMACS and other remote sensing and in situ measurements during HALO–$(\mathcal{AC})^3$.

2 Data and methods

2.1 Measurements

The data used in this work were collected during the airborne HALO–$(\mathcal{AC})^3$ measurement campaign in the Arctic (Wendisch et al., 2024; Ehrlich et al., 2025). The German research aircraft HALO was equipped with remote sensing instrumentation and followed a quasi-Lagrangian sampling strategy. In addition, several research flights were performed in coordination with the Polar 5 and Polar 6 aircraft (Wesche et al., 2016), containing remote sensing and in situ instrumentation. This work, however, focuses on data from HALO.

The analyses presented in the following sections are based on measurements of the spectrometer of the Munich Aerosol Cloud Scanner (specMACS, Ewald et al., 2016; Weber et al., 2024), which was operated in a downward-looking configuration on board HALO. specMACS consists of two hyperspectral cameras (so-called VNIR and SWIR), which are sensitive to the visible and near-infrared wavelength range between 400 nm and 2500 nm, and two 2D RGB polarization-resolving cameras. The SWIR spectrometer used in this work has a field of view of 35.3 ° in across-track direction, and the polarization resolving cameras have a maximum combined field of view of $91° \times 117°$ in along-track and across-track direction, respectively. The different components of specMACS provide high-spatial resolution measurements of macrophysical and microphysical properties of clouds with spatial resolutions between 10 m and 100 m for typical flight altitudes (10 km), depending on the retrieved quantity.

Macrophysical cloud properties that can be derived from the measurements include the cloud top height, the cloud fraction, and the horizontal extent of the clouds. The cloud top height is obtained from a stereographic retrieval using a method by Kölling et al. (2019), and the cloud fraction is calculated from the brightness-based cloud mask from Pörtge et al. (2023). The horizontal cloud extent is derived from the retrieved 3D cloud geometry using the watershedding algorithm implemented in the Tracking and Object-Based Analysis of Clouds (TOBAC) package (Heikenfeld et al., 2019; Sokolowsky et al., 2024). The algorithm provides the horizontal area of the identified cloud elements from which an effective cloud radius was calculated by assuming a circular shape.

Moreover, specMACS provides measurements of microphysical cloud properties. The effective radius of liquid cloud droplets is computed with the multi-angle polarimetric cloudbow retrieval by Pörtge et al. (2023). Information about the cloud thermodynamic phase is derived from the specMACS measurements following two different approaches. Firstly, the spectral ice index defined by Ehrlich et al. (2008) and Ruiz-Donoso et al. (2020) was calculated from the measurements of the SWIR spectrometer. The ice index is a qualitative measure of the thermodynamic phase. Values smaller than 20 indicate a liquid water cloud and larger values correspond to a mixed-phase cloud (Ehrlich et al., 2009). Secondly, a quantitative optical ice fraction was

https://doi.org/10.5194/egusphere-2025-5831
Preprint. Discussion started: 28 November 2025

derived from the measurements of the polarization-resolving cameras by applying the polarimetric phase partitioning retrieval introduced by Weber et al. (2025b). The ice fraction is defined as the ratio of the ice optical thickness to the total cloud optical thickness. Here, the results of the polarimetric phase retrieval for the cloudbow angular range using the IDEFAX forward operator for the green color channel are shown and only observations with saturated polarization signals are considered, because they provide the smallest uncertainties (Weber et al., 2025b). For more details to the phase retrieval, the reader is refered to Weber et al. (2025b). Nevertheless, the results have a high uncertainty, especially when the solar zenith angle is very large. The microphysical cloud properties derived from specMACS observations are representative for the cloud top as they are based on passive remote sensing. The spectral measurements used to calculate the ice index originate from deeper layers within the cloud than the polarization measurements applied to compute the ice fraction and the effective radius of the liquid cloud droplets, since the polarization signal is dominated by single scattering.

Only measurements above open ocean were considered. Over sea ice, the retrievals based on passive remote sensing have additional uncertainties due to the influence of the surface, especially for thin clouds. In addition, it is difficult to detect clouds above sea ice correctly. Thus, a sea ice mask was computed from the combined AMSR2-MODIS sea ice dataset (Ludwig et al., 2020). All observations and measurements with sea ice concentrations larger than 80 %, which is a typical choice for the definition of the sea ice edge, were excluded from further analysis. At this threshold value, sea ice still partially affects the measurements, but cloud formation begins as soon as small fractions of open ocean are present, and this initial phase should not be excluded from the analyses.

2.2 Backward trajectories

To study the evolution of cloud properties during the observed MCAOs in a quasi-Lagrangian framework, measurements and retrieval results were combined with backward trajectories, which allow to assign every measurement the time or distance the airmass has traveled southwards since passing the ice edge. The backward trajectories were computed from ERA5 wind fields using Lagranto (Sprenger and Wernli, 2015). Every 1 min along each HALO flight track, a trajectory was initialized horizontally at the location of HALO, and vertically at 920 hPa pressure altitude, which roughly corresponds to cloud top. The trajectories were calculated backwards for 24 hours also tracing the sea ice concentration (SIC) from the combined AMSR2-MODIS dataset (Ludwig et al., 2020). The obtained backward trajectories have an improved reliability as the dropsondes released from the HALO aircraft have been assimilated in ERA5. The trajectories cover comparably short timescales and therefore the influence of errors remains small (Kirbus et al., 2024).

The time and distance the airmass traveled above open ocean was computed for every trajectory by integrating the fraction of open water (1 - SIC) over time and distance, similar to Spensberger and Spengler (2021). For better comparability, the evolution of the cloud properties is analyzed both as a function of time and distance above open ocean, as some studies use time while others use distance. In addition, the wind speed is not constant along the trajectories.

https://doi.org/10.5194/egusphere-2025-5831
Preprint. Discussion started: 28 November 2025

2.3 Overview of the research flights

During HALO–$(\mathcal{AC})^3$, MCAOs were sampled that evolved in different synoptic situations (Walbröl et al., 2024). Between 2022-03-21 and the end of the campaign on 2022-04-12, a long cold phase with several MCAOs occurred. Especially strong MCAO events, exceeding the 90th and 75th percentiles of the MCAO index climatology, were observed on 2022-03-25 and 2022-04-02, respectively (Walbröl et al., 2024). The strength of the MCAOs can be characterized through the MCAO index, which is defined as the difference of the potential skin temperature at the surface and the potential temperature at a pressure of 850 hPa (Fletcher et al., 2016)

$$M_{\mathrm{CAO}} = \theta_{\mathrm{skin}} - \theta_{850\mathrm{hPa}}. \tag{1}$$

Larger differences are related to more intense MCAOs. MCAOs with indices indicating temperature differences between $0\,\mathrm{K} < M_{\mathrm{CAO}} < 4\,\mathrm{K}$ are typically refered to as weak events, whereas MCAOs with $4\,\mathrm{K} < M_{\mathrm{CAO}} < 8\,\mathrm{K}$ and $M_{\mathrm{CAO}} > 8\,\mathrm{K}$ can be classified as moderate and strong events, respectively (Papritz and Spengler, 2017; Dahlke et al., 2022).

HALO conducted six flights during the cold phase of the campaign, which targeted MCAOs. An overview of the flights analyzed here is given in Fig. 1, where MODIS satellite images and the flight tracks are shown for the research flights on 2022-03-21, 2022-03-28, 2022-03-29, 2022-03-30, 2022-04-01, and 2022-04-04. The research flights covered mostly the Fram Strait region, but for example on 2022-03-29 the area south-east of Svalbard was sampled. Some parts of the flights are affected by the topography of the island of Svalbard, causing, e.g., convergence lines downstream. The long cold period led to increasing sea ice extent north and south-east of Svalbard. The flight patterns mostly followed the quasi-Lagrangian sampling approach with flight legs oriented perpendicular to and along the wind direction (Wendisch et al., 2024). The strength of the observed MCAOs varied between the different research flights. The mean and maximum values of the MCAO index along the flight tracks of all research flights computed from ERA5 data (Hersbach et al., 2023a, b) are summarized in Table 1. The strongest observed MCAO events were on 2022-04-01 and on 2022-03-29. Weaker MCAO conditions were, for example, measured on 2022-03-30. In addition, the flights sampled different parts of the MCAOs. For example, the research flight on 2022-04-01 focused on the very initial phase of the MCAO, whereas the other research flights also covered regions further downstream. Thus, different parts of the temporal and spatial evolution were sampled.

The quasi-Lagrangian flight strategy applied to all flights of the HALO–$(\mathcal{AC})^3$ campaign (Wendisch et al., 2024) allows for studying the evolution of cloud properties during the observed MCAOs. Specifically, the temporal and spatial evolution of macroscopic cloud properties, such as the cloud top height, cloud fraction, and horizontal cloud extent, as well as the evolution of cloud microphysical properties, such as the effective radius of liquid water droplets and cloud thermodynamic phase partitioning, will be analyzed in the following.

https://doi.org/10.5194/egusphere-2025-5831
Preprint. Discussion started: 28 November 2025

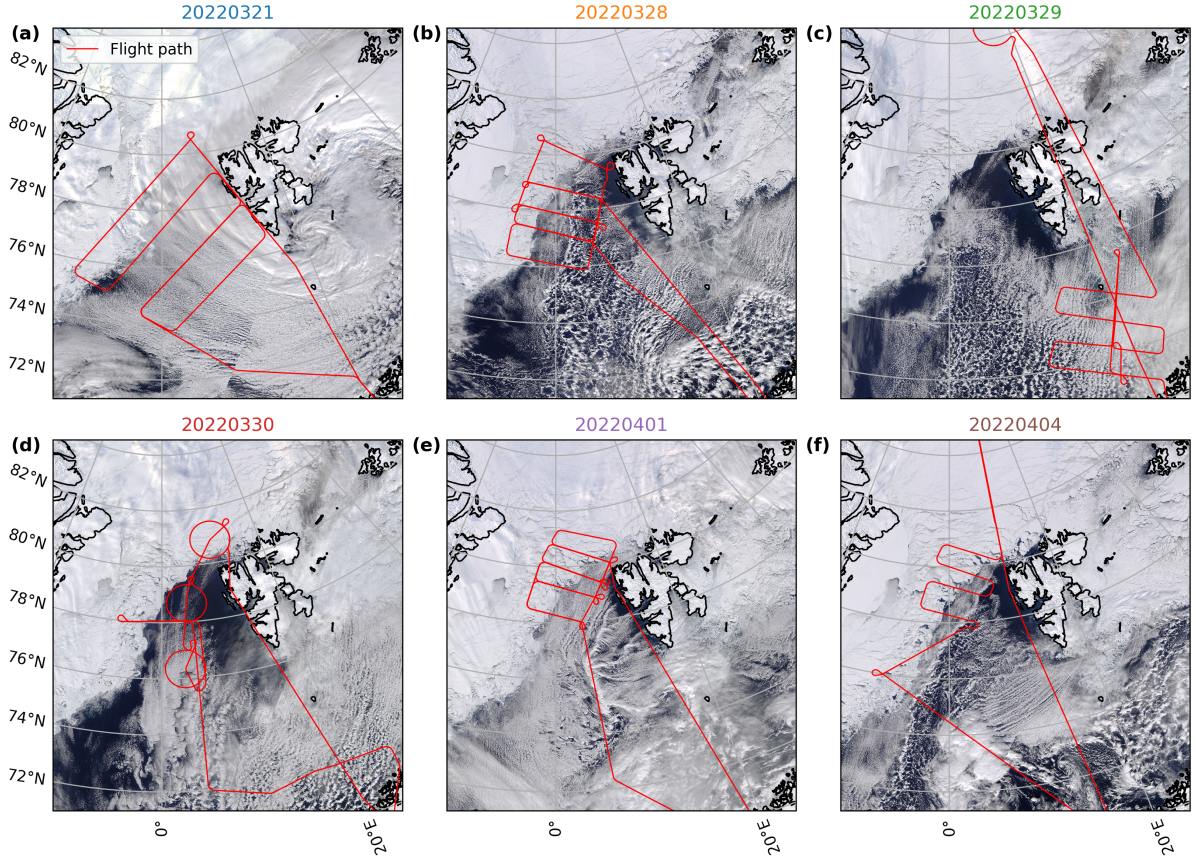

Figure 1. MODIS satellite images (Corrected Reflectance (True Color)) from NASA Worldview (https://worldview.earthdata.nasa.gov/) for all MCAO flights of HALO–$(\mathcal{AC})^3$. The red lines indicate the flight tracks.

Table 1. Mean and maximum MCAO indices along flight track computed from ERA5 data (Hersbach et al., 2023a, b) for all MCAO flights of HALO–$(\mathcal{AC})^3$. The colors correspond to the colors of the research flights in Fig. 5 and 6.

Research flight	Mean MCAO index [K]	Maximum MCAO index [K]
20220321	1.91	7.62
20220328	3.28	7.35
20220329	5.32	9.23
20220330	0.44	3.25
20220401	6.59	11.85
20220404	1.89	7.51

https://doi.org/10.5194/egusphere-2025-5831
Preprint. Discussion started: 28 November 2025

3 Results

3.1 Case study: MCAO on 2022-04-01

As a case study, the data collected on the research flight conducted by HALO on 2022-04-01 are analyzed first. The flight sampled the initial phase of a MCAO in the Fram Strait (see Fig. 1e). Average and maximum MCAO indices along the flight track of about 7 K and 12 K (see Table 1) classify this case as a moderate to strong event. It appears as a typical event for the Fram Strait region during that time of the year (Kirbus et al., 2024). The satellite image in Fig. 1e shows cloud streets oriented along the mean wind direction from the ice edge towards the south to south-west. The thermodynamic evolution during this MCAO was studied by Kirbus et al. (2024), based on dropsonde measurements during HALO–$(\mathcal{AC})^3$. In addition, Schirmacher et al. (2024) investigated the roll convection regime using radar observations. In the following, the temporal and spatial evolution of the macrophysical and microphysical cloud properties, including the cloud top height, cloud thermodynamic phase, and cloud droplet size will be presented and discussed.

3.1.1 Evolution of macrophysical cloud properties

First, the temporal and spatial evolution of the macrophysical cloud properties is analyzed for the flight on 2022-04-01. To this end, the cloud top height, the cloud fraction, and the cloud radius were derived from the specMACS measurements and combined with backward trajectories as described in Sect. 2.

Figure 2 shows the cloud top height (left column), cloud fraction (middle column), and cloud radius (right column) as a function of time (upper row) and distance (lower row) the airmass traveled above open ocean. The histograms for every time or distance bin are normalized by the total number of observations of the respective bin. In addition, Figure 3 displays RGB images taken by the polarization-resolving cameras at four points in time (about 30 min, 60 min, 90 min, and 150 min above open ocean) to illustrate the observed cloud morphology. Parts of Fig. 2 and 3 have also been shown in Wendisch et al. (2024).

The cloud top height in Fig. 2a and 2d increases stepwise and almost linearly with time and distance from about 250 m close to the ice edge to about 1.5 km after 300 min. This increase of cloud top height with time is typical for the evolution of clouds during MCAOs as the ABL deepens with time (Murray-Watson et al., 2023; Kirbus et al., 2024). The cloud fraction (see Fig. 2b and 2e) remained almost constant during the first hours of the observed MCAO as can also be seen in the RGB images in Fig. 3. Cloud fractions close to unity are observed at very small distances and times above open ocean. These high cloud fractions are due to the misidentification of bright sea ice in the marginal ice zone as clouds by the cloud mask, which is based on the brightness. In contrast, Murray-Watson et al. (2023) found increasing cloud fractions during the first hours of MCAOs followed by a slight decrease and generally slightly higher cloud fraction values. However, they used satellite observations with a much coarser spatial resolution of 25 km compared to the high spatial resolution of 10 m to 100 m of the airborne specMACS observations, and the cloud fraction strongly depends on the threshold values applied in the cloud mask.

Finally, the cloud radius increases from approximately 0.5 km to 1 km, with high variability. These results agree with the increasing roll circulation wavelength from initially 1 km to 2 km derived from data measured by the radar installed on the

https://doi.org/10.5194/egusphere-2025-5831
Preprint. Discussion started: 28 November 2025

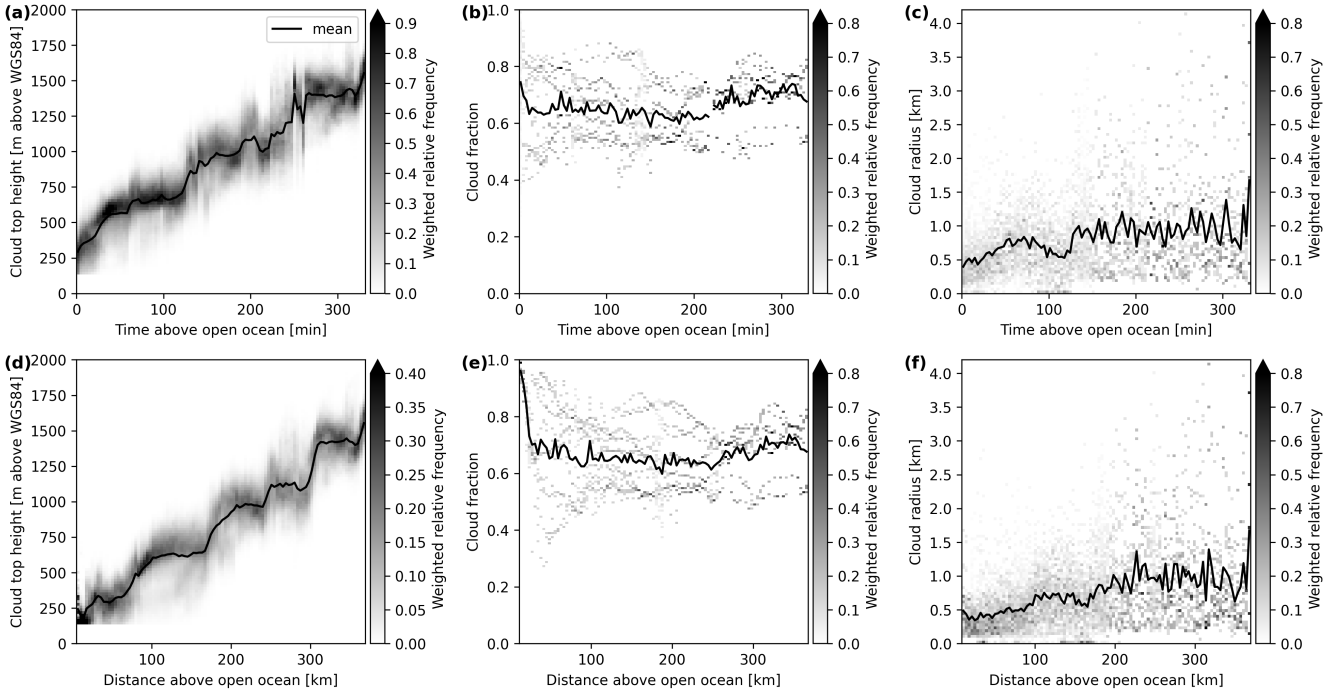

Figure 2. Histograms of cloud top height **(a, d)**, cloud fraction **(b, e)**, and cloud radius **(c, f)** as a function of time (upper row) and distance (lower row) above open ocean. The black line indicates the mean.

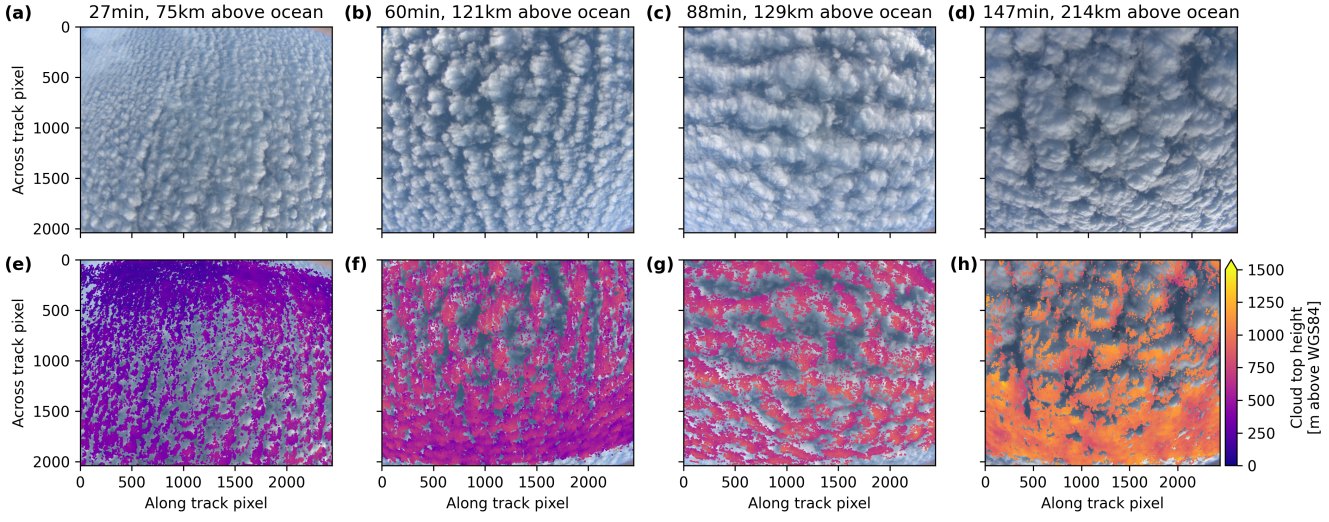

Figure 3. Example RGB images (upper row) and cloud top heights (lower row) at four different points in time, about 30 min, 60 min, 90 min, and 150 min above open ocean.

https://doi.org/10.5194/egusphere-2025-5831
Preprint. Discussion started: 28 November 2025

Polar 5 aircraft on the same day and in the same region (Schirmacher et al., 2024). The cloud radius distribution consists of a mixture of smaller and larger clouds (see Fig. 3).

The different shapes of the curves describing, e.g., the evolution of the cloud top height during the first kilometers above open ocean compared to the first minutes above open ocean in Fig. 2 can be explained by changing wind speeds due to the off-ice acceleration at the sea ice edge. Moreover, the RGB images in Fig. 3 show cloud streets in panels (a) to (c), which are commonly observed in the initial phase of a MCAO (Brümmer, 1999). After about 150 min, more cellular structures evolve that are visible in panel (d), indicating a transition of cloud morphology from the cloud streets towards a cellular cloud regime.

3.1.2 Cloud microphysical properties

The same analysis as for the macrophysical quantities was also performed for microphysical cloud characteristics such as the effective radius of liquid water droplets and the cloud thermodynamic phase, quantified through the ice index and ice fraction. Figure 4 displays the evolution of the effective radius of the liquid water droplets (a, d), the ice index (b, e), and the ice fraction (c, f) as a function of time and distance above open ocean. For later times (after approx. 210 min), no measurements of the effective radius and the ice fraction are available because the solar zenith angle during this part of the flight was too large for the cloudbow to be inside the field of view of the cameras.

The effective radius of liquid cloud droplets shows a rapid increase from about 5 µm to 7.5 µm in the first approximately 30 min. It remains then constant until about 150 min above open ocean, even though the cloud top height increases with time throughout the observed time period, which is usually accompanied by an increase in droplet size. At the same time, the ice index indicates the presence of ice crystals. Hence, the constant effective radius during this time could be explained by ice crystals competing with the cloud droplets for the available water vapor, limiting the growth of liquid cloud droplets on the one hand, or freezing of larger cloud droplets on the other hand. Afterward, the effective radius becomes more variable and increases slightly, which coincides with the transition from cloud streets to cellular structures. In the more convective cellular regime, liquid water is formed in the convective updrafts at the centers of the cells, which could lead to further increasing effective radii at the higher cloud tops (Schirmacher et al., 2024; Maherndl et al., 2024). However, the number of measurements is also smaller in this time range due to larger solar zenith angles, and the results are therefore more uncertain. The spike in the evolution of the effective radius at very small distances in panel (d) is due to the influence of sea ice, which was not completely filtered out and should be treated as an outlier. The uncertainty of the measured effective radii of liquid cloud droplets from the cloudbow retrieval is $-0.2 \pm 1.6\,\mu\mathrm{m}$, based on an evaluation with synthetic data (Volkmer et al., 2024; Pörtge, 2024). Therefore, the observed increase of the liquid cloud droplet size is outside the range of uncertainties.

The evolution of the effective radius of liquid cloud droplets during MCAOs was also studied by Murray-Watson et al. (2023), who found increasing effective radii with time and larger sizes between about 12 µm and 18 µm. The effective radii were, however, derived from MODIS satellite data with a bispectral retrieval, which has large uncertainties for Arctic mixed-phase clouds and a much coarser spatial resolution. In addition, they focused on liquid water clouds only. In situ measurements of the effective radius conducted by the Polar 6 aircraft during the same day and in the same region show average effective radii of about 4 µm during the first 100 min above open ocean and slightly increasing radii for larger times (Moser et al.,

https://doi.org/10.5194/egusphere-2025-5831
Preprint. Discussion started: 28 November 2025

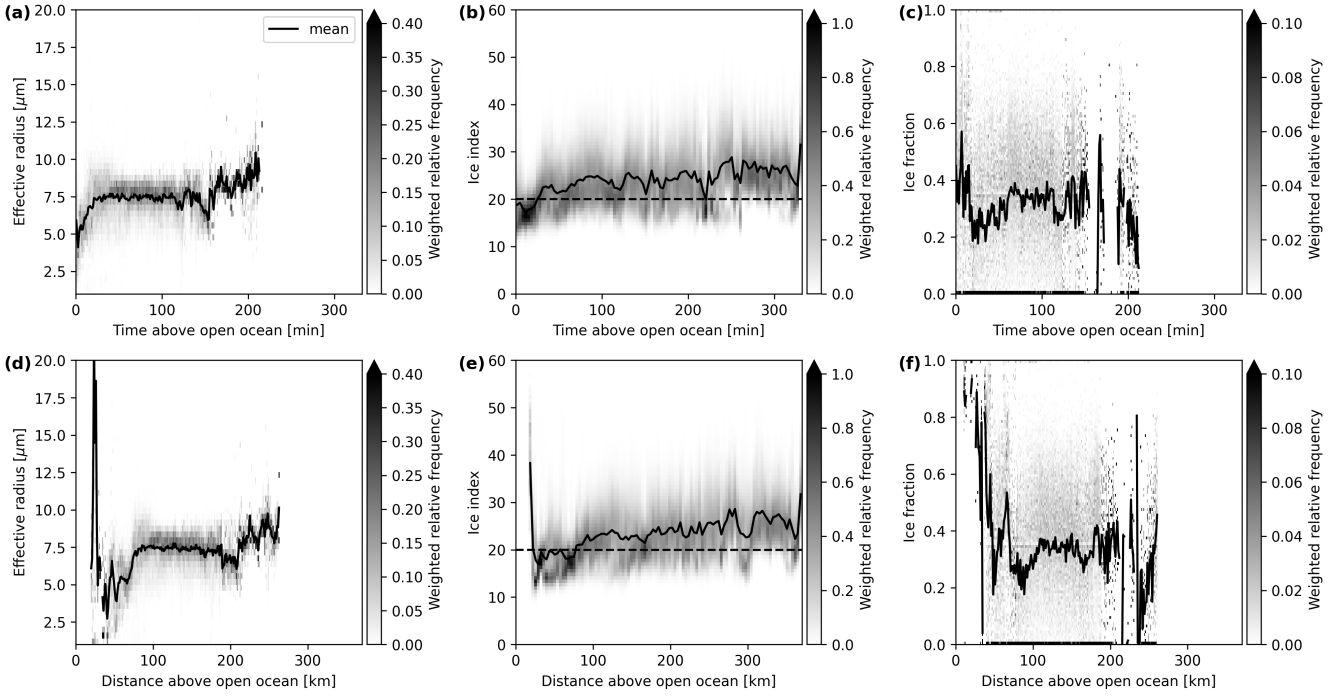

Figure 4. Histograms of the effective radius of the liquid water droplets **(a, d)**, the ice index **(b, e)**, and the ice fraction **(c, f)** as a function of time (upper row) and distance (lower row) above open ocean. The black solid line indicates the mean, the black dashed line in panels **(b)** and **(e)** is the threshold value between the liquid water and the mixed phase.

2023). While the effective radii derived from cloudbow observations of specMACS are representative for cloud top, the Polar 6 aircraft was flying lower inside the cloud. This could explain the slightly smaller observed values of the in situ measurements compared to the cloudbow retrieval results.

The evolution of cloud thermodynamic phase is studied using the spectral ice index and the ice fractions from the polarized phase retrieval in the middle and right columns of Fig. 4, respectively. The results of the multi-angle polarimetric retrieval of the ice fraction and the spectral approach applied to derive the ice index have different penetration depths. Both are representative for the cloud top, but the spectral signal originates from slightly deeper altitudes within the cloud than the polarized signal. The ice index is smaller than 20 during the first 30 min, indicating a pure liquid water cloud. Subsequently, it transforms into a mixed-phase cloud with slightly increasing ice indices over time. The transition from pure liquid water to the mixed phase occurs during the same time range as the rapid increase of the effective radius at the beginning. Larger effective radii increase the probability for freezing of liquid water droplets and heterogeneous ice formation. In addition, during the same time range, the cloud top height increased and the cloud top temperature decreased. Thus, a threshold temperature and size of the cloud liquid water droplets could be reached that initiate the formation of ice crystals.

https://doi.org/10.5194/egusphere-2025-5831
Preprint. Discussion started: 28 November 2025

The evolution of the ice fraction shows a similar structure. The higher ice fractions close to the sea ice edge are caused by a misclassification of sea ice as cloud. The cloud mask using the spectral data is more accurate here, as a wavelength of 1640 nm is applied, where sea ice is comparably dark. The cloud mask for the polarized retrieval is more affected by sea ice. Considering the initially high ice fraction as outliers and taking the bias of the ice fraction for the cloudbow range into account (Weber et al., 2025b), the ice fraction at the beginning was in the range of 0.2. It then increases until about 90 min above open ocean and stays almost constant, but the cloud top is still dominated by liquid water. The initially faster decrease of the ice fraction appears slightly later than the increase of the spectral ice index, which is more sensitive to ice and representative for slightly lower altitudes, deeper within the cloud. From around 150 min above open ocean, when the transition from cloud streets to cells was observed, the ice fraction becomes variable but also uncertain.

3.2 Statistics of all six MCAOs

After studying the temporal and spatial evolution of cloud macrophysical and microphysical properties during the MCAO on 2022-04-01, the analyses are extended to all research flights targeting MCAOs. The different observed MCAOs cover a variety of different conditions, as discussed in Sect. 2.3. This allows to further investigate the variability of the cloud evolution between different events and the dependence on the strength of the MCAO.

3.2.1 Evolution of macrophysical cloud properties

Similar to above, the temporal and spatial evolution of the macrophysical cloud properties is analyzed first. To this end, the cloud top height, the cloud fraction, and the cloud radius were derived from the specMACS measurements and combined with backward trajectories as described in Sect. 2 for all research flights. Figure 5 displays histograms of these quantities as a function of time (upper row) and distance (lower row) above open ocean together with their mean for all flights in different colors. The first, second, and third columns correspond to the cloud top height, cloud fraction, and cloud radius, respectively. In general, there is a large variability between the different research flights, which were performed under varying MCAO conditions and partly in different regions.

The cloud top height in panels (a) and (d) increases with time and distance from the ice edge for all research flights from a few hundred meters to a maximum of about 2.5 km. The largest cloud top heights are observed during the flights on 2022-04-01 (purple line) and 2022-03-29 (green line), which were the strongest observed MCAOs, and lower cloud top heights are reached during the weaker MCAOs. In addition, the increase is faster for these strong events compared to the weaker ones. Larger cloud top heights for stronger MCAOs were also observed by Murray-Watson et al. (2023) and Schirmacher et al. (2024). The very large cloud top heights on 2022-03-21 at large times and distances are due to high-level cirrus clouds south-west of Svalbard, as can also be seen in Fig. 1a.

A similar picture is found for the horizontal cloud extent in Fig. 5c and 5f. The cloud radius generally increases with time and distance above open ocean from a few hundred meters to about 1.5 km. Larger cloud radii are associated with the stronger events on 2022-04-01 and 2022-03-29, and smaller radii are observed during the weaker events on 2022-04-04, 2022-03-30,

https://doi.org/10.5194/egusphere-2025-5831
Preprint. Discussion started: 28 November 2025

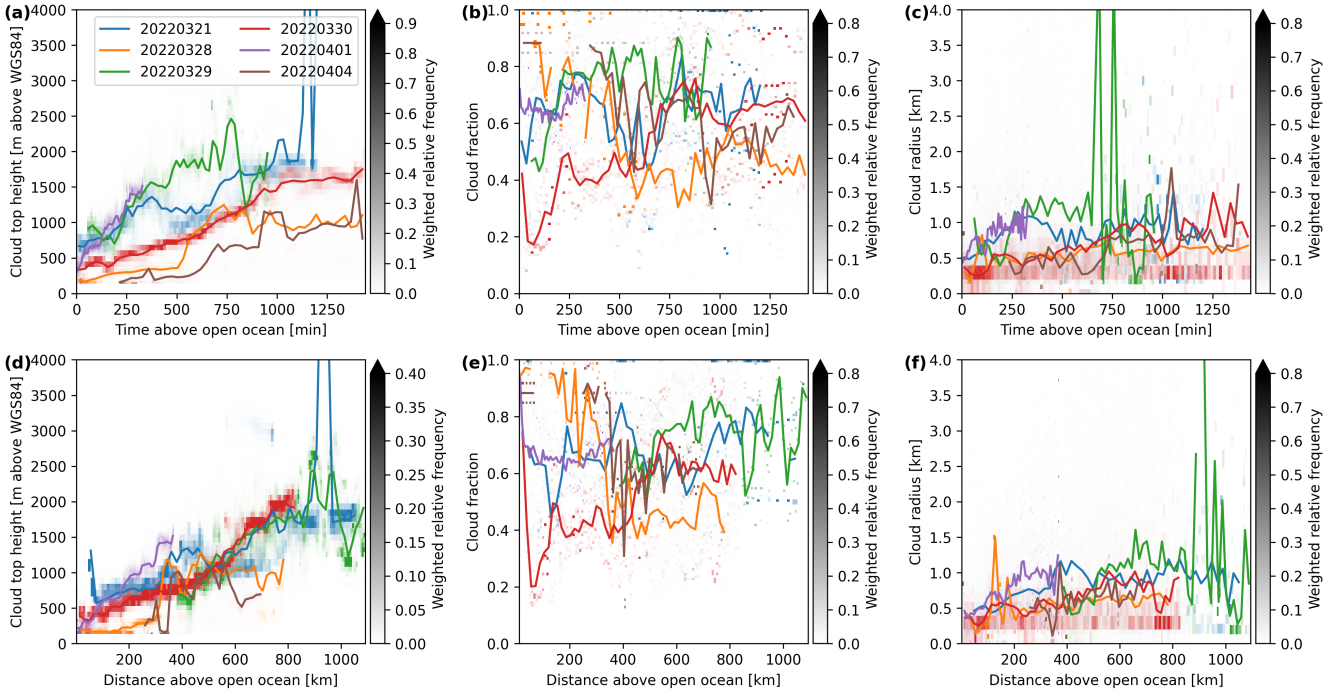

Figure 5. Histograms of cloud top height **(a, d)**, cloud fraction **(b, e)**, and cloud radius **(c, f)** as a function of time (upper row) and distance (lower row) above open ocean with their respective mean for all MCAO flights during HALO–$(\mathcal{AC})^3$. The different colors correspond to the different research flights and the solid lines denote the respective means.

and 2022-03-28. Similar to the cloud top height, the increase of the cloud radius is faster for stronger events than for weaker MCAOs.

In contrast, the cloud fraction shows a more complicated behavior and a large variability. Cloud fractions close to 1 are observed at very small distances and times above open ocean. These high cloud fractions are due to the misidentification of bright sea ice in the marginal ice zone as clouds by the cloud mask, as discussed above. In addition, there are some island effects affecting cloud cover (see Fig. 1). In general, the cloud fraction remains either relatively constant or increases with time, with typical values between 0.4 and 0.8. The stronger MCAOs in Fig. 5 tend to have larger cloud fractions compared to the weaker ones. This agrees with the observations of larger cloud fractions during the first hours of MCAOs for stronger events by Murray-Watson et al. (2023). The flight on 2022-03-28 is an exception and strongly affected by the local topography of Svalbard.

3.2.2 Evolution of microphysical cloud properties

Similar to the macrophysical cloud properties, the temporal and spatial evolution of cloud microphysical properties and their variability and dependence on the MCAO strength are investigated by combining measurements with backward trajectories, as

https://doi.org/10.5194/egusphere-2025-5831
Preprint. Discussion started: 28 November 2025

in the previous sections. Figure 6 displays the effective radius of liquid cloud droplets, the ice index, and the ice fraction in the first, second, and third column, respectively, as a function of time (upper row) and distance (lower row) above open ocean.

The effective radius of liquid cloud droplets increases with time and distance above open ocean, and sizes between about 3 µm and 17 µm were observed. Larger effective radii are reached during the stronger events on 2022-04-01 and 2022-03-29, for which the growth of the cloud droplets is also faster. This can be expected as the effective radius in general increases with height within a cloud, and larger cloud top heights were observed for stronger MCAOs in Fig. 5. In contrast, Murray-Watson et al. (2023) found also increasing effective radii with time, but smaller effective radii for stronger MCAOs compared to weaker events. However, they focused on liquid-dominated clouds only and the retrieved effective radii from satellite observations are much more uncertain and have a much coarser spatial resolution than the effective radii derived with the polarimetric cloudbow retrieval.

Concerning the cloud thermodynamic phase, the ice indices and ice fractions generally increase with time above open ocean. The patterns of both ice index and ice fraction are very similar. Initial values of the ice index are below or around 20, which is the threshold value between liquid water and mixed-phase clouds, and increase to about 30 to 50, depending on the research flight. In addition, the ice fraction increases with time and distance from very small values around 0.2 to approximately 0.5 to 0.8. The ice fraction is overestimated at very small times and distances close to the ice edge due to the misclassification of sea ice in the marginal ice zone as clouds. The large variability of both the ice index and ice fraction also reflects the larger uncertainty in the thermodynamic phase retrievals compared to the stereographic or the cloudbow retrieval. The described increase in the ice index and ice fraction indicates a transition from a liquid water to a mixed-phase regime with increasing amounts of ice. This phase transition is faster for the stronger observed MCAOs on 2022-04-01, 2022-03-29, and 2022-03-21. In addition, stronger events reach higher ice indices and ice fractions. The faster phase transition and higher ice fractions for stronger events agree with the higher observed cloud top heights and larger effective radii for these events, since typically colder temperatures at higher altitudes and larger cloud droplets increase the probability of ice formation, which typically happens through heterogeneous freezing (de Boer et al., 2011; Cui et al., 2006; Ansmann et al., 2005). Similar to the case study of the MCAO on 2022-04-01, the phase transition coincides with an increase of the effective radius of the liquid cloud droplets and increasing cloud top heights during all observed cases.

4 Discussion and conclusions

In this work, the spatial and temporal evolution of macrophysical and microphysical cloud properties during the initial phase of marine cold air outbreaks in the Arctic was studied with a focus on cloud thermodynamic phase partitioning and phase transitions. To this end, quasi-Lagrangian airborne passive remote sensing observations with specMACS during the HALO–$(\mathcal{AC})^3$ campaign in the Arctic were combined with backward trajectories. The evolution of cloud macrophysical and microphysical properties was analyzed for all flights targeting MCAOs and compared to investigate also the variability of the cloud evolution and the dependence on the MCAO strength.

https://doi.org/10.5194/egusphere-2025-5831
Preprint. Discussion started: 28 November 2025

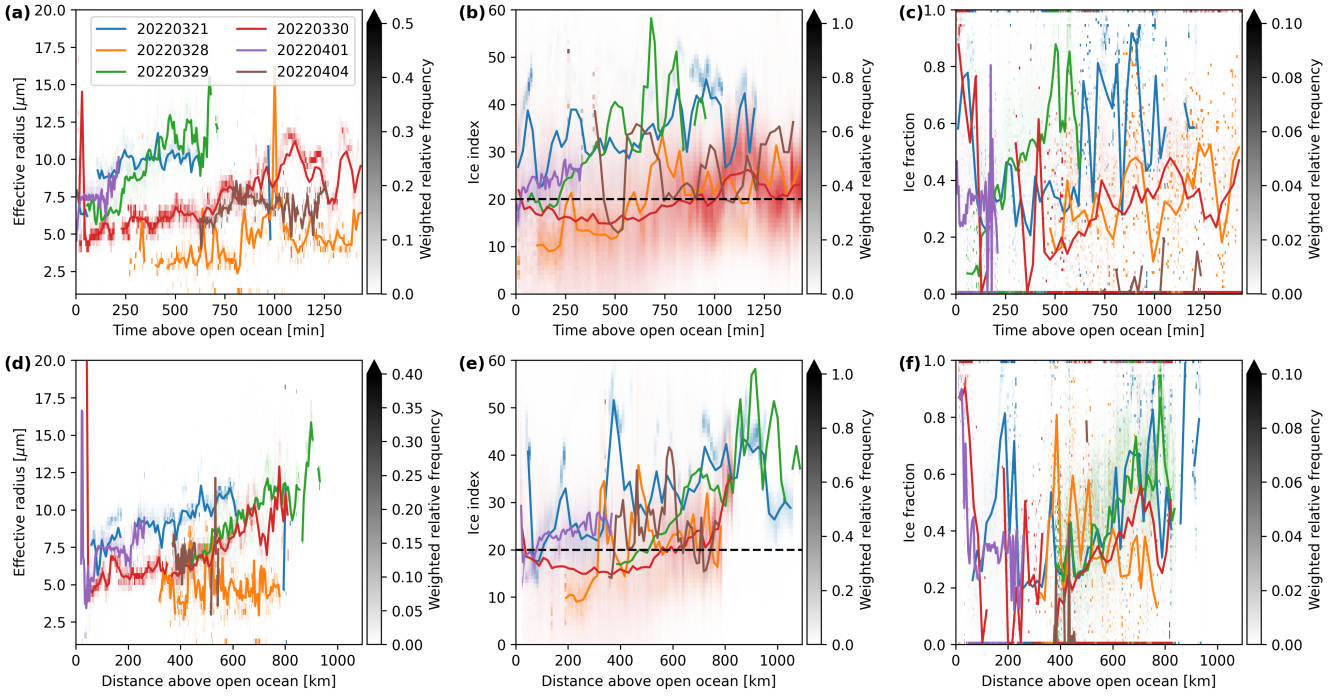

Figure 6. Histograms of effective radius of liquid cloud droplets **(a, d)**, ice index **(b, e)**, and ice fraction **(c, f)** as a function of time (upper row) and distance (lower row) above open ocean for all MCAO flights of HALO–$(\mathcal{AC})^3$, The solid lines indicate the mean of the respective flight, the black dashed line in panels **(b)** and **(e)** is the threshold value between the liquid water and the mixed phase.

A case study of a strong MCAO on 2022-04-01 showed increasing cloud top heights and horizontal cloud extents with increasing time and distance above open ocean, while the cloud fraction stayed almost constant during the observed first five hours of the MCAO. Moreover, the effective radius of liquid water droplets increased from about 5 µm to 7.5 µm during the first approximately 30 min and remained constant afterward. This initial increase of the effective radius coincided with an increase of the ice index and ice fraction and a transition from a pure liquid water to a mixed-phase cloud regime.

The same analysis was repeated for all six observed MCAOs. The cloud top heights and horizontal extents increased with time and distance traveled above open ocean during all MCAOs. However, the increase was stronger and faster for more intense MCAOs. Similarly, the effective radius of liquid cloud droplets increased over time and reached larger sizes for stronger MCAOs. Furthermore, increasing ice indices and ice fractions with time and a transition from an initially liquid water to a mixed-phase regime were observed during all MCAOs. This transition happened earlier for stronger MCAO, and larger ice indices and ice fractions were reached for the stronger events. In all observed cases, the transition from the liquid water to the mixed phase coincided with an increase of the effective radius of the liquid cloud droplets and the cloud top height. As the ABL and clouds evolve and the cloud top height increases, the liquid cloud droplets grow to larger sizes and the cloud top temperature typically decreases, leading to an increasing probability of ice formation through heterogeneous freezing. In general,

https://doi.org/10.5194/egusphere-2025-5831
Preprint. Discussion started: 28 November 2025

a large variability was observed between the different MCAO cases measured during HALO–$(\mathcal{AC})^3$. The measurements were performed in partly different regions, with different MCAO strengths, different parts of the evolution were sampled, and some island effects also affected the measurements. Only a small number of six MCAO could be studied, which, however, covered a large range of MCAO conditions (Walbröl et al., 2024).

Some limitations of the presented results should be considered. The brightness-based cloud mask for the polarization-resolving cameras of specMACS struggles in the presence of sea ice, where ice can falsely be identified as clouds. This is a known issue for cloud masks based on passive imaging methods. Thus, an improved cloud mask should be developed in the future to improve the results of the analyses. In addition, the large solar zenith angles in the Arctic lead to increased uncertainties of the retrievals of the specMACS instrument. On the one hand, three-dimensional radiative effects have a stronger influence on the phase retrievals for large solar zenith angles. On the other hand, the cloudbow is then observed at the edge of the field of view of the polarization-resolving cameras, where the measurement uncertainties are larger (Weber et al., 2024). The results of the cloudbow retrieval and the polarized phase partitioning retrieval were filtered, excluding for example retrieval results with a large root mean square error between the fitted model and the measurement, to eliminate the most uncertain results.

Furthermore, it should be mentioned that the definition of the ice fraction varies strongly between different studies, depending on the type of measurements and the application (Korolev et al., 2017). In addition, different threshold values are used to define the liquid water, mixed, and ice phase. This must be kept in mind when comparing the results of different studies on phase partitioning. In this work, the ice fraction is an optical ice fraction defined by the optical thickness, and the ice index is a qualitative measure of cloud thermodynamic phase.

The quasi-Lagrangian airborne measurements applied in this work complement satellite-based studies as they have a much higher spatial resolution and additional cloud properties, such as cloud thermodynamic phase partitioning, can be studied. The observations of the temporal and spatial evolution of cloud macrophysical and micropyhsical properties during the initial phase of MCAOs presented in this work provide unique observational data, which could be used for model evaluation in the future. Mixed-phase clouds, their thermodynamic phase partitioning, and their evolution during meridional airmass transformations, such as MCAOs, are not well represented in models. The presented observations could be compared to model results in a Eulerian and a quasi-Lagrangian way for the six observed MCAOs, similar to Wendisch et al. (2025) who analyzed the thermodynamic evolution of MCAOs in dropsonde observations and in the ICON weather prediction model. Furthermore, based on the analyses of the temporal and spatial evolution of clouds during MCAOs during HALO–$(\mathcal{AC})^3$, the vertical cloud structure and its evolution during a MCAO is investigated in the second part of this work in Weber et al. (2025a).

In the analyses presented in this work, the MCAOs were distinguished in terms of their strength, quantified through the MCAO index. Besides the MCAO intensity, the aerosol concentration also affects the evolution of cloud properties (Murray-Watson et al., 2023) and was not considered so far. The effect of aerosols on the cloud properties could be further studied in the future, using, for example, collocated in situ measurements and lidar observations on board HALO during HALO–$(\mathcal{AC})^3$ to characterize the aerosol conditions.

https://doi.org/10.5194/egusphere-2025-5831
Preprint. Discussion started: 28 November 2025

Code and data availability. The data collected during the HALO–$(AC)^3$ campaign are published on PANGAEA (Ehrlich et al., 2025). The measurements of the SWIR camera of specMACS are available at Weber et al. (2024). Retrieval results from specMACS, the HALO backward trajectories, and the analysis codes used in this work can be provided upon request from the corresponding author.

Author contributions. AW evaluated all data, performed the analyses, and wrote the manuscript with input from all co-athours. BK computed the backward trajectories. MW and BM provided valuable feedback to the analyses and the outline of the study. All authors contributed to the discussion of the results.

Competing interests. Bernhard Mayer is member of the editorial board of AMT.

Acknowledgements. We would like to thank Fabian Hoffmann for valuable discussions about cloud microphysics. In addition, we thank Lea Volkmer for applying the stereographic retrieval to the specMACS observations and thank the entire HALO–$(AC)^3$ team involved in the realization of the measurement flights and the data processing. Furthermore, we thank the Institute of Environmental Physics, University of Bremen for the provision of the merged MODIS-AMSR2 sea-ice concentration data at https://data.seaice.uni-bremen.de/modis_amsr2 (last access 2023-09-18). We are further grateful for funding of project grant no. 316646266 and 442667104 by the Deutsche Forschungsgemeinschaft (DFG, German Research Foundation) within the framework of Priority Programme SPP 1294 to promote research with HALO. Furthermore, we appreciate the funding provided by DFG – Project-ID 268020496 – TRR 172.

https://doi.org/10.5194/egusphere-2025-5831
Preprint. Discussion started: 28 November 2025

References

Abel, S. J., Boutle, I. A., Waite, K., Fox, S., Brown, P. R. A., Cotton, R., Lloyd, G., Choularton, T. W., and Bower, K. N.: The Role of Precipitation in Controlling the Transition from Stratocumulus to Cumulus Clouds in a Northern Hemisphere Cold-Air Outbreak, Journal of the Atmospheric Sciences, 74, 2293 – 2314, https://doi.org/10.1175/JAS-D-16-0362.1, 2017.

Ahn, E., Huang, Y., Siems, S. T., and Manton, M. J.: A Comparison of Cloud Microphysical Properties Derived From MODIS and CALIPSO With In Situ Measurements Over the Wintertime Southern Ocean, Journal of Geophysical Research: Atmospheres, 123, 11,120–11,140, https://doi.org/10.1029/2018JD028535, 2018.

Ansmann, A., Mattis, I., Müller, D., Wandinger, U., Radlach, M., Althausen, D., and Damoah, R.: Ice formation in Saharan dust over central Europe observed with temperature/humidity/aerosol Raman lidar, J. Geophys. Res., 110, https://doi.org/10.1029/2004JD005000, 2005.

Block, K., Schneider, F. A., Mülmenstädt, J., Salzmann, M., and Quaas, J.: Climate models disagree on the sign of total radiative feedback in the Arctic, Tellus A: Dynamic Meteorology and Oceanography, 2020.

Boettcher, M., Schäfler, A., Sprenger, M., Sodemann, H., Kaufmann, S., Voigt, C., Schlager, H., Summa, D., Di Girolamo, P., Nerini, D., Germann, U., and Wernli, H.: Lagrangian matches between observations from aircraft, lidar and radar in a warm conveyor belt crossing orography, Atmospheric Chemistry and Physics, 21, 5477–5498, https://doi.org/10.5194/acp-21-5477-2021, 2021.

Brümmer, B.: Boundary-layer modification in wintertime cold-air outbreaks from the Arctic sea ice, Boundary-Layer Meteorology, 80, 109–125, https://doi.org/10.1007/BF00119014, 1996.

Brümmer, B.: Roll and Cell Convection in Wintertime Arctic Cold-Air Outbreaks, Journal of the Atmospheric Sciences, 56, 2613 – 2636, https://doi.org/10.1175/1520-0469(1999)056<2613:RACCIW>2.0.CO;2, 1999.

Cesana, G., Waliser, D. E., Jiang, X., and Li, J.-L. F.: Multimodel evaluation of cloud phase transition using satellite and reanalysis data, Journal of Geophysical Research: Atmospheres, 120, 7871–7892, https://doi.org/10.1002/2014JD022932, 2015.

Cesana, G. V., Khadir, T., Chepfer, H., and Chiriaco, M.: Southern Ocean Solar Reflection Biases in CMIP6 Models Linked to Cloud Phase and Vertical Structure Representations, Geophysical Research Letters, 49, e2022GL099 777, https://doi.org/10.1029/2022GL099777, e2022GL099777 2022GL099777, 2022.

Choi, Y.-S., Ho, C.-H., Park, C.-E., Storelvmo, T., and Tan, I.: Influence of cloud phase composition on climate feedbacks, Journal of Geophysical Research: Atmospheres, 119, 3687–3700, https://doi.org/10.1002/2013JD020582, 2014.

Cohen, J., Zhang, X., Francis, J., Jung, T., Kwok, R., Overland, J., Ballinger, T. J., Bhatt, U. S., Chen, H. W., Coumou, D., Feldstein, S., Gu, H., Handorf, D., Henderson, G., Ionita, M., Kretschmer, M., Laliberte, F., Lee, S., Linderholm, H. W., Maslowski, W., Peings, Y., Pfeiffer, K., Rigor, I., Semmler, T., Stroeve, J., Taylor, P. C., Vavrus, S., Vihma, T., Wang, S., Wendisch, M., Wu, Y., and Yoon, J.: Divergent consensuses on Arctic amplification influence on midlatitude severe winter weather, Nature Climate Change, 10, 20–29, https://doi.org/10.1038/s41558-019-0662-y, 2020.

Cui, Z., Carslaw, K. S., Yin, Y., and Davies, S.: A numerical study of aerosol effects on the dynamics and microphysics of a deep convective cloud in a continental environment, Journal of Geophysical Research: Atmospheres, 111, https://doi.org/10.1029/2005JD005981, 2006.

Dahlke, S., Solbès, A., and Maturilli, M.: Cold Air Outbreaks in Fram Strait: Climatology, Trends, and Observations During an Extreme Season in 2020, Journal of Geophysical Research: Atmospheres, 127, e2021JD035 741, https://doi.org/10.1029/2021JD035741, e2021JD035741 2021JD035741, 2022.

de Boer, G., Morrison, H., Shupe, M. D., and Hildner, R.: Evidence of liquid dependent ice nucleation in high-latitude stratiform clouds from surface remote sensors, Geophysical Research Letters, 38, https://doi.org/10.1029/2010GL046016, 2011.

https://doi.org/10.5194/egusphere-2025-5831
Preprint. Discussion started: 28 November 2025

Ehrlich, A., Bierwirth, E., Wendisch, M., Gayet, J.-F., Mioche, G., Lampert, A., and Heintzenberg, J.: Cloud phase identification of Arctic boundary-layer clouds from airborne spectral reflection measurements: test of three approaches, Atmospheric Chemistry and Physics, 8, 7493–7505, https://doi.org/10.5194/acp-8-7493-2008, 2008.

Ehrlich, A., Wendisch, M., Bierwirth, E., Gayet, J.-F., Mioche, G., Lampert, A., and Mayer, B.: Evidence of ice crystals at cloud top of Arctic boundary-layer mixed-phase clouds derived from airborne remote sensing, Atmospheric Chemistry and Physics, 9, 9401–9416, https://doi.org/10.5194/acp-9-9401-2009, 2009.

Ehrlich, A., Crewell, S., Herber, A., Klingebiel, M., Lüpkes, C., Mech, M., Becker, S., Borrmann, S., Bozem, H., Buschmann, M., Clemen, H.-C., De La Torre Castro, E., Dorff, H., Dupuy, R., Eppers, O., Ewald, F., George, G., Giez, A., Grawe, S., Gourbeyre, C., Hartmann, J., Jäkel, E., Joppe, P., Jourdan, O., Jurányi, Z., Kirbus, B., Lucke, J., Luebke, A. E., Maahn, M., Maherndl, N., Mallaun, C., Mayer, J., Mertes, S., Mioche, G., Moser, M., Müller, H., Pörtge, V., Risse, N., Roberts, G., Rosenburg, S., Röttenbacher, J., Schäfer, M., Schaefer, J., Schäfler, A., Schirmacher, I., Schneider, J., Schnitt, S., Stratmann, F., Tatzelt, C., Voigt, C., Walbröl, A., Weber, A., Wetzel, B., Wirth, M., and Wendisch, M.: A comprehensive in situ and remote sensing data set collected during the HALO–$(\mathcal{AC})^3$ aircraft campaign, Earth System Science Data, 17, 1295–1328, https://doi.org/10.5194/essd-17-1295-2025, 2025.

Ewald, F., Kölling, T., Baumgartner, A., Zinner, T., and Mayer, B.: Design and characterization of specMACS, a multipurpose hyperspectral cloud and sky imager, Atmospheric Measurement Techniques, 9, 2015–2042, https://doi.org/10.5194/amt-9-2015-2016, 2016.

Field, P. R., Cotton, R. J., McBeath, K., Lock, A. P., Webster, S., and Allan, R. P.: Improving a convection-permitting model simulation of a cold air outbreak, Quarterly Journal of the Royal Meteorological Society, 140, 124–138, https://doi.org/10.1002/qj.2116, 2014.

Field, P. R., Brozkova, R., Chen, M., Dudhia, J., Lac, C., Hara, T., Honnert, R., Olson, J., Siebesma, P., de Roode, S., Tomassini, L., Hill, A., and McTaggart-Cowan, R.: Exploring the convective grey zone with regional simulations of a cold air outbreak, Quarterly Journal of the Royal Meteorological Society, 143, 2537–2555, https://doi.org/10.1002/qj.3105, 2017.

Fletcher, J., Mason, S., and Jakob, C.: The Climatology, Meteorology, and Boundary Layer Structure of Marine Cold Air Outbreaks in Both Hemispheres, Journal of Climate, 29, 1999 – 2014, https://doi.org/10.1175/JCLI-D-15-0268.1, 2016.

Forsberg, R., Hvidegaard, S. M., Skourup, H., and Simonsen, S.: Three decades of polar airborne campaigns in the Arctic and Antarctica, in: AGU Fall Meeting Abstracts, vol. 2023 of *AGU Fall Meeting Abstracts*, pp. C31C–1365, 2023.

Geerts, B., Giangrande, S. E., McFarquhar, G. M., Xue, L., Abel, S. J., Comstock, J. M., Crewell, S., DeMott, P. J., Ebell, K., Field, P., Hill, T. C. J., Hunzinger, A., Jensen, M. P., Johnson, K. L., Juliano, T. W., Kollias, P., Kosovic, B., Lackner, C., Luke, E., Lüpkes, C., Matthews, A. A., Neggers, R., Ovchinnikov, M., Powers, H., Shupe, M. D., Spengler, T., Swanson, B. E., Tjernström, M., Theisen, A. K., Wales, N. A., Wang, Y., Wendisch, M., and Wu, P.: The COMBLE Campaign: A Study of Marine Boundary Layer Clouds in Arctic Cold-Air Outbreaks, Bulletin of the American Meteorological Society, 103, E1371 – E1389, https://doi.org/10.1175/BAMS-D-21-0044.1, 2022.

Gryschka, M. and Raasch, S.: Roll convection during a cold air outbreak: A large eddy simulation with stationary model domain, Geophysical Research Letters, 32, https://doi.org/10.1029/2005GL022872, 2005.

Heikenfeld, M., Marinescu, P. J., Christensen, M., Watson-Parris, D., Senf, F., van den Heever, S. C., and Stier, P.: tobac 1.2: towards a flexible framework for tracking and analysis of clouds in diverse datasets, Geoscientific Model Development, 12, 4551–4570, https://doi.org/10.5194/gmd-12-4551-2019, 2019.

Hersbach, H., Bell, B., Berrisford, P., Biavati, G., Horányi, A., Muñoz Sabater, J., Nicolas, J., Peubey, C., Radu, R., Rozum, I., Schepers, D., Simmons, A., Soci, C., Dee, D., and Thépaut, J.-N.: ERA5 hourly data on pressure levels from 1940 to present, https://doi.org/10.24381/cds.bd0915c6, accessed on 2025-04-03, 2023a.

https://doi.org/10.5194/egusphere-2025-5831
Preprint. Discussion started: 28 November 2025

Hersbach, H., Bell, B., Berrisford, P., Biavati, G., Horányi, A., Muñoz Sabater, J., Nicolas, J., Peubey, C., Radu, R., Rozum, I., Schepers, D., Simmons, A., Soci, C., Dee, D., and Thépaut, J.-N.: ERA5 hourly data on single levels from 1940 to present, https://doi.org/10.24381/cds.adbb2d47, accessed on 2025-04-03, 2023b.

Inoue, J., Sato, K., Rinke, A., Cassano, J. J., Fettweis, X., Heinemann, G., Matthes, H., Orr, A., Phillips, T., Seefeldt, M., Solomon, A., and Webster, S.: Clouds and Radiation Processes in Regional Climate Models Evaluated Using Observations Over the Ice-free Arctic Ocean, Journal of Geophysical Research: Atmospheres, 126, e2020JD033 904, https://doi.org/10.1029/2020JD033904, e2020JD033904 2020JD033904, 2021.

Kirbus, B., Schirmacher, I., Klingebiel, M., Schäfer, M., Ehrlich, A., Slättberg, N., Lucke, J., Moser, M., Müller, H., and Wendisch, M.: Thermodynamic and cloud evolution in a cold-air outbreak during HALO-(AC)^3: quasi-Lagrangian observations compared to the ERA5 and CARRA reanalyses, Atmospheric Chemistry and Physics, 24, 3883–3904, https://doi.org/10.5194/acp-24-3883-2024, 2024.

Kölling, T., Zinner, T., and Mayer, B.: Aircraft-based stereographic reconstruction of 3-D cloud geometry, Atmospheric Measurement Techniques, 12, 1155–1166, https://doi.org/10.5194/amt-12-1155-2019, 2019.

Komurcu, M., Storelvmo, T., Tan, I., Lohmann, U., Yun, Y., Penner, J. E., Wang, Y., Liu, X., and Takemura, T.: Intercomparison of the cloud water phase among global climate models, Journal of Geophysical Research: Atmospheres, 119, 3372–3400, https://doi.org/10.1002/2013JD021119, 2014.

Korolev, A. and Milbrandt, J.: How Are Mixed-Phase Clouds Mixed?, Geophysical Research Letters, 49, e2022GL099 578, https://doi.org/10.1029/2022GL099578, e2022GL099578 2022GL099578, 2022.

Korolev, A., McFarquhar, G., Field, P. R., Franklin, C., Lawson, P., Wang, Z., Williams, E., Abel, S. J., Axisa, D., Borrmann, S., Crosier, J., Fugal, J., Krämer, M., Lohmann, U., Schlenczek, O., Schnaiter, M., and Wendisch, M.: Mixed-Phase Clouds: Progress and Challenges, Meteorological Monographs, 58, 5.1 – 5.50, https://doi.org/10.1175/AMSMONOGRAPHS-D-17-0001.1, 2017.

Krautstrunk, M. and Giez, A.: The Transition From FALCON to HALO Era Airborne Atmospheric Research, pp. 609–624, Springer Berlin Heidelberg, Berlin, Heidelberg, https://doi.org/10.1007/978-3-642-30183-4_37, 2012.

Kretzschmar, J., Salzmann, M., Mülmenstädt, J., and Quaas, J.: Arctic clouds in ECHAM6 and their sensitivity to cloud microphysics and surface fluxes, Atmospheric Chemistry and Physics, 19, 10 571–10 589, https://doi.org/10.5194/acp-19-10571-2019, 2019.

Kretzschmar, J., Stapf, J., Klocke, D., Wendisch, M., and Quaas, J.: Employing airborne radiation and cloud microphysics observations to improve cloud representation in ICON at kilometer-scale resolution in the Arctic, Atmospheric Chemistry and Physics, 20, 13 145–13 165, https://doi.org/10.5194/acp-20-13145-2020, 2020.

Lackner, C. P., Geerts, B., Juliano, T. W., Xue, L., and Kosovic, B.: Vertical Structure of Clouds and Precipitation During Arctic Cold-Air Outbreaks and Warm-Air Intrusions: Observations From COMBLE, Journal of Geophysical Research: Atmospheres, 128, e2022JD038 403, https://doi.org/10.1029/2022JD038403, e2022JD038403 2022JD038403, 2023.

Lloyd, G., Choularton, T. W., Bower, K. N., Gallagher, M. W., Crosier, J., O'Shea, S., Abel, S. J., Fox, S., Cotton, R., and Boutle, I. A.: In situ measurements of cloud microphysical and aerosol properties during the break-up of stratocumulus cloud layers in cold air outbreaks over the North Atlantic, Atmospheric Chemistry and Physics, 18, 17 191–17 206, https://doi.org/10.5194/acp-18-17191-2018, 2018.

Ludwig, V., Spreen, G., and Pedersen, L. T.: Evaluation of a New Merged Sea-Ice Concentration Dataset at 1 km Resolution from Thermal Infrared and Passive Microwave Satellite Data in the Arctic, Remote Sensing, 12, https://doi.org/10.3390/rs12193183, 2020.

Mages, Z., Kollias, P., Zhu, Z., and Luke, E. P.: Surface-based observations of cold-air outbreak clouds during the COMBLE field campaign, Atmospheric Chemistry and Physics, 23, 3561–3574, https://doi.org/10.5194/acp-23-3561-2023, 2023.

https://doi.org/10.5194/egusphere-2025-5831
Preprint. Discussion started: 28 November 2025

Maherndl, N., Moser, M., Schirmacher, I., Bansemer, A., Lucke, J., Voigt, C., and Maahn, M.: How does riming influence the observed spatial variability of ice water in mixed-phase clouds?, Atmospheric Chemistry and Physics, 24, 13 935–13 960, https://doi.org/10.5194/acp-24-13935-2024, 2024.

Marchant, B., Platnick, S., Meyer, K., and Wind, G.: Evaluation of the MODIS Collection 6 multilayer cloud detection algorithm through comparisons with CloudSat Cloud Profiling Radar and CALIPSO CALIOP products, Atmospheric Measurement Techniques, 13, 3263–3275, https://doi.org/10.5194/amt-13-3263-2020, 2020.

Mateling, M. E., Pettersen, C., Kulie, M. S., and L'Ecuyer, T. S.: Marine Cold-Air Outbreak Snowfall in the North Atlantic: A CloudSat Perspective, Journal of Geophysical Research: Atmospheres, 128, e2022JD038 053, https://doi.org/10.1029/2022JD038053, e2022JD038053 2022JD038053, 2023.

Matus, A. V. and L'Ecuyer, T. S.: The role of cloud phase in Earth's radiation budget, Journal of Geophysical Research: Atmospheres, 122, 2559–2578, https://doi.org/10.1002/2016JD025951, 2017.

McCoy, D. T., Hartmann, D. L., Zelinka, M. D., Ceppi, P., and Grosvenor, D. P.: Mixed-phase cloud physics and Southern Ocean cloud feedback in climate models, Journal of Geophysical Research: Atmospheres, 120, 9539–9554, https://doi.org/10.1002/2015JD023603, 2015.

McCoy, I. L., Wood, R., and Fletcher, J. K.: Identifying Meteorological Controls on Open and Closed Mesoscale Cellular Convection Associated with Marine Cold Air Outbreaks, Journal of Geophysical Research: Atmospheres, 122, 11,678–11,702, https://doi.org/10.1002/2017JD027031, 2017.

Michaelis, J., Schmitt, A. U., Lüpkes, C., Hartmann, J., Birnbaum, G., and Vihma, T.: Observations of marine cold-air outbreaks: a comprehensive data set of airborne and dropsonde measurements from the Springtime Atmospheric Boundary Layer Experiment (STABLE), Earth System Science Data, 14, 1621–1637, https://doi.org/10.5194/essd-14-1621-2022, 2022.

Morrison, H., De Boer, G., Feingold, G., Harrington, J., Shupe, M., and Sulia, K.: Resilience of persistent Arctic mixed-phase clouds, Nature Geoscience, 5, 11–17, https://doi.org/10.1038/ngeo1332, 2012.

Moser, M., Lucke, J., De La Torre Castro, E., Mayer, J., and Voigt, C.: DLR in situ cloud measurements during HALO-(AC)^3 Arctic airborne campaign, https://doi.org/10.1594/PANGAEA.963247, 2023.

Murray-Watson, R. J., Gryspeerdt, E., and Goren, T.: Investigating the development of clouds within marine cold-air outbreaks, Atmospheric Chemistry and Physics, 23, 9365–9383, https://doi.org/10.5194/acp-23-9365-2023, 2023.

Papritz, L. and Spengler, T.: A Lagrangian Climatology of Wintertime Cold Air Outbreaks in the Irminger and Nordic Seas and Their Role in Shaping Air–Sea Heat Fluxes, Journal of Climate, 30, 2717 – 2737, https://doi.org/10.1175/JCLI-D-16-0605.1, 2017.

Pithan, F., Medeiros, B., and Mauritsen, T.: Mixed-phase clouds cause climate model biases in Arctic wintertime temperature inversions, Climate Dynamics, https://doi.org/10.1007/s00382-013-1964-9, 2014.

Pithan, F., Ackerman, A., Angevine, W. M., Hartung, K., Ickes, L., Kelley, M., Medeiros, B., Sandu, I., Steeneveld, G.-J., Sterk, H. A. M., Svensson, G., Vaillancourt, P. A., and Zadra, A.: Select strengths and biases of models in representing the Arctic winter boundary layer over sea ice: the Larcform 1 single column model intercomparison, Journal of Advances in Modeling Earth Systems, 8, 1345–1357, https://doi.org/10.1002/2016MS000630, 2016.

Pithan, F., Svensson, G., Caballero, R., Chechin, D., Cronin, T. W., Ekman, A. M. L., Neggers, R., Shupe, M. D., Solomon, A., Tjernström, M., and Wendisch, M.: Role of air-mass transformations in exchange between the Arctic and mid-latitudes, Nature Geoscience, 11, 805–812, https://doi.org/10.1038/s41561-018-0234-1, 2018.

https://doi.org/10.5194/egusphere-2025-5831
Preprint. Discussion started: 28 November 2025

Pörtge, V., Kölling, T., Weber, A., Volkmer, L., Emde, C., Zinner, T., Forster, L., and Mayer, B.: High-spatial-resolution retrieval of cloud droplet size distribution from polarized observations of the cloudbow, Atmospheric Measurement Techniques, 16, 645–667, https://doi.org/10.5194/amt-16-645-2023, 2023.

Pörtge, V. T.: Understanding cloud droplet size distributions from multi-angle polarimetric observations, http://nbn-resolving.de/urn:nbn:de:bvb:19-340021, 2024.

Ruiz-Donoso, E., Ehrlich, A., Schäfer, M., Jäkel, E., Schemann, V., Crewell, S., Mech, M., Kulla, B. S., Kliesch, L.-L., Neuber, R., and Wendisch, M.: Small-scale structure of thermodynamic phase in Arctic mixed-phase clouds observed by airborne remote sensing during a cold air outbreak and a warm air advection event, Atmospheric Chemistry and Physics, 20, 5487–5511, https://doi.org/10.5194/acp-20-5487-2020, 2020.

Sato, Y., Miura, H., Yashiro, H., Goto, D., Takemura, T., Tomita, H., and Nakajima, T.: Unrealistically pristine air in the Arctic produced by current global scale models, Scientific Reports, 6, https://doi.org/10.1038/srep26561, 2016.

Schäfer, M., Bierwirth, E., Ehrlich, A., Jäkel, E., Werner, F., and Wendisch, M.: Directional, horizontal inhomogeneities of cloud optical thickness fields retrieved from ground-based and airbornespectral imaging, Atmospheric Chemistry and Physics, 17, 2359–2372, https://doi.org/10.5194/acp-17-2359-2017, 2017.

Schäfer, M., Loewe, K., Ehrlich, A., Hoose, C., and Wendisch, M.: Simulated and observed horizontal inhomogeneities of optical thickness of Arctic stratus, Atmospheric Chemistry and Physics, 18, 13 115–13 133, https://doi.org/10.5194/acp-18-13115-2018, 2018.

Schirmacher, I., Schnitt, S., Klingebiel, M., Maherndl, N., Kirbus, B., Ehrlich, A., Mech, M., and Crewell, S.: Clouds and precipitation in the initial phase of marine cold-air outbreaks as observed by airborne remote sensing, Atmospheric Chemistry and Physics, 24, 12 823–12 842, https://doi.org/10.5194/acp-24-12823-2024, 2024.

Seppala, H., Zhang, Z., and Zheng, X.: Developing a Lagrangian Frame Transformation on Satellite Data to Study Cloud Microphysical Transitions in Arctic Marine Cold Air Outbreaks, Geophysical Research Letters, 52, e2025GL115 637, https://doi.org/10.1029/2025GL115637, e2025GL115637 2025GL115637, 2025.

Shupe, M. D., Rex, M., Blomquist, B., Persson, P. O. G., Schmale, J., Uttal, T., Althausen, D., Angot, H., Archer, S., Bariteau, L., Beck, I., Bilberry, J., Bucci, S., Buck, C., Boyer, M., Brasseur, Z., Brooks, I. M., Calmer, R., Cassano, J., Castro, V., Chu, D., Costa, D., Cox, C. J., Creamean, J., Crewell, S., Dahlke, S., Damm, E., de Boer, G., Deckelmann, H., Dethloff, K., Dütsch, M., Ebell, K., Ehrlich, A., Ellis, J., Engelmann, R., Fong, A. A., Frey, M. M., Gallagher, M. R., Ganzeveld, L., Gradinger, R., Graeser, J., Greenamyer, V., Griesche, H., Griffiths, S., Hamilton, J., Heinemann, G., Helmig, D., Herber, A., Heuzé, C., Hofer, J., Houchens, T., Howard, D., Inoue, J., Jacobi, H.-W., Jaiser, R., Jokinen, T., Jourdan, O., Jozef, G., King, W., Kirchgaessner, A., Klingebiel, M., Krassovski, M., Krumpen, T., Lampert, A., Landing, W., Laurila, T., Lawrence, D., Lonardi, M., Loose, B., Lüpkes, C., Maahn, M., Macke, A., Maslowski, W., Marsay, C., Maturilli, M., Mech, M., Morris, S., Moser, M., Nicolaus, M., Ortega, P., Osborn, J., Pätzold, F., Perovich, D. K., Petäjä, T., Pilz, C., Pirazzini, R., Posman, K., Powers, H., Pratt, K. A., Preußer, A., Quéléver, L., Radenz, M., Rabe, B., Rinke, A., Sachs, T., Schulz, A., Siebert, H., Silva, T., Solomon, A., Sommerfeld, A., Spreen, G., Stephens, M., Stohl, A., Svensson, G., Uin, J., Viegas, J., Voigt, C., von der Gathen, P., Wehner, B., Welker, J. M., Wendisch, M., Werner, M., Xie, Z., and Yue, F.: Overview of the MOSAiC expedition: Atmosphere, Elementa: Science of the Anthropocene, 10, 00 060, https://doi.org/10.1525/elementa.2021.00060, 2022.

Smith, D. M., Screen, J. A., Deser, C., Cohen, J., Fyfe, J. C., García-Serrano, J., Jung, T., Kattsov, V., Matei, D., Msadek, R., Peings, Y., Sigmond, M., Ukita, J., Yoon, J.-H., and Zhang, X.: The Polar Amplification Model Intercomparison Project (PAMIP) contribution to CMIP6: investigating the causes and consequences of polar amplification, Geoscientific Model Development, 12, 1139–1164, https://doi.org/10.5194/gmd-12-1139-2019, 2019.

https://doi.org/10.5194/egusphere-2025-5831
Preprint. Discussion started: 28 November 2025

Sokolowsky, G. A., Freeman, S. W., Jones, W. K., Kukulies, J., Senf, F., Marinescu, P. J., Heikenfeld, M., Brunner, K. N., Bruning, E. C., Collis, S. M., Jackson, R. C., Leung, G. R., Pfeifer, N., Raut, B. A., Saleeby, S. M., Stier, P., and van den Heever, S. C.: *tobac* v1.5: introducing fast 3D tracking, splits and mergers, and other enhancements for identifying and analysing meteorological phenomena, Geoscientific Model Development, 17, 5309–5330, https://doi.org/10.5194/gmd-17-5309-2024, 2024.

Spensberger, C. and Spengler, T.: Sensitivity of Air-Sea Heat Exchange in Cold-Air Outbreaks to Model Resolution and Sea-Ice Distribution, Journal of Geophysical Research: Atmospheres, 126, e2020JD033 610, https://doi.org/https://doi.org/10.1029/2020JD033610, e2020JD033610 2020JD033610, 2021.

Sprenger, M. and Wernli, H.: The LAGRANTO Lagrangian analysis tool – version 2.0, Geoscientific Model Development, 8, 2569–2586, https://doi.org/10.5194/gmd-8-2569-2015, 2015.

Stevens, B., Ament, F., Bony, S., Crewell, S., Ewald, F., Gross, S., Hansen, A., Hirsch, L., Jacob, M., Kölling, T., Konow, H., Mayer, B., Wendisch, M., Wirth, M., Wolf, K., Bakan, S., Bauer-Pfundstein, M., Brueck, M., Delanoë, J., Ehrlich, A., Farrell, D., Forde, M., Gödde, F., Grob, H., Hagen, M., Jäkel, E., Jansen, F., Klepp, C., Klingebiel, M., Mech, M., Peters, G., Rapp, M., Wing, A. A., and Zinner, T.: A High-Altitude Long-Range Aircraft Configured as a Cloud Observatory: The NARVAL Expeditions, Bulletin of the American Meteorological Society, 100, 1061 – 1077, https://doi.org/10.1175/BAMS-D-18-0198.1, 2019.

Svingen, K., Brakstad, A., Våge, K., von Appen, W.-J., and Papritz, L.: The Impact of Cold-Air Outbreaks and Oceanic Lateral Fluxes on Dense-Water Formation in the Greenland Sea from a 10-Year Moored Record (1999–2009), Journal of Physical Oceanography, 53, 1499 – 1517, https://doi.org/10.1175/JPO-D-22-0160.1, 2023.

Tan, I. and Storelvmo, T.: Evidence of Strong Contributions From Mixed-Phase Clouds to Arctic Climate Change, Geophysical Research Letters, 46, 2894–2902, https://doi.org/10.1029/2018GL081871, 2019.

Tomassini, L., Field, P. R., Honnert, R., Malardel, S., McTaggart-Cowan, R., Saitou, K., Noda, A. T., and Seifert, A.: The "Grey Zone" cold air outbreak global model intercomparison: A cross evaluation using large-eddy simulations, Journal of Advances in Modeling Earth Systems, 9, 39–64, https://doi.org/10.1002/2016MS000822, 2017.

Tornow, F., Ackerman, A. S., and Fridlind, A. M.: Preconditioning of overcast-to-broken cloud transitions by riming in marine cold air outbreaks, Atmospheric Chemistry and Physics, 21, 12 049–12 067, https://doi.org/10.5194/acp-21-12049-2021, 2021.

Tornow, F., Ackerman, A. S., Fridlind, A. M., Tselioudis, G., Cairns, B., Painemal, D., and Elsaesser, G.: On the Impact of a Dry Intrusion Driving Cloud-Regime Transitions in a Midlatitude Cold-Air Outbreak, Journal of the Atmospheric Sciences, 80, 2881 – 2896, https://doi.org/10.1175/JAS-D-23-0040.1, 2023.

Uttal, T., Curry, J. A., McPhee, M. G., Perovich, D. K., Moritz, R. E., Maslanik, J. A., Guest, P. S., Stern, H. L., Moore, J. A., Turenne, R., Heiberg, A., Serreze, M. C., Wylie, D. P., Persson, O. G., Paulson, C. A., Halle, C., Morison, J. H., Wheeler, P. A., Makshtas, A., Welch, H., Shupe, M. D., Intrieri, J. M., Stamnes, K., Lindsey, R. W., Pinkel, R., Pegau, W. S., Stanton, T. P., and Grenfeld, T. C.: Surface Heat Budget of the Arctic Ocean, Bulletin of the American Meteorological Society, 83, 255 – 276, https://doi.org/10.1175/1520-0477(2002)083<0255:SHBOTA>2.3.CO;2, 2002.

Volkmer, L., Pörtge, V., Jakub, F., and Mayer, B.: Model-based evaluation of cloud geometry and droplet size retrievals from two-dimensional polarized measurements of specMACS, Atmospheric Measurement Techniques, 17, 1703–1719, https://doi.org/10.5194/amt-17-1703-2024, 2024.

Walbröl, A., Michaelis, J., Becker, S., Dorff, H., Ebell, K., Gorodetskaya, I., Heinold, B., Kirbus, B., Lauer, M., Maherndl, N., Maturilli, M., Mayer, J., Müller, H., Neggers, R. A. J., Paulus, F. M., Röttenbacher, J., Rückert, J. E., Schirmacher, I., Slättberg, N., Ehrlich, A., Wendisch,

https://doi.org/10.5194/egusphere-2025-5831
Preprint. Discussion started: 28 November 2025

M., and Crewell, S.: Contrasting extremely warm and long-lasting cold air anomalies in the North Atlantic sector of the Arctic during the HALO-$(\mathcal{AC})^3$ campaign, Atmospheric Chemistry and Physics, 24, 8007–8029, https://doi.org/10.5194/acp-24-8007-2024, 2024.

Weber, A., Kölling, T., Pörtge, V., Baumgartner, A., Rammeloo, C., Zinner, T., and Mayer, B.: Polarization upgrade of specMACS: calibration and characterization of the 2D RGB polarization-resolving cameras, Atmospheric Measurement Techniques, 17, 1419–1439, https://doi.org/10.5194/amt-17-1419-2024, 2024.

Weber, A., Pörtge, V., Zinner, T., and Mayer, B.: Spectral radiance measurements with the hyperspectral and polarized imaging system specMACS during the HALO-(AC)3 field campaign, https://doi.org/10.1594/PANGAEA.966992, 2024.

Weber, A., Hoffmann, F., and Mayer, B.: Quasi-Lagrangian observations of cloud transitions during the initial phase of marine cold air outbreaks in the Arctic – Part 2: Vertical cloud structure, submitted to ACP, 2025a.

Weber, A., Pörtge, V., Emde, C., and Mayer, B.: Retrieval of cloud thermodynamic phase partitioning from multi-angle polarimetric imaging of Arctic mixed-phase clouds, EGUsphere, 2025, 1–28, https://doi.org/10.5194/egusphere-2025-3595, 2025b.

Wendisch, M., Handorf, D., Tegen, I., Neggers, R. A. J., and Spreen, G.: Glimpsing the Ins and Outs of the Arctic Atmospheric Cauldron, Eos, 102, https://doi.org/10.1029/2021EO155959, 2021.

Wendisch, M., Brückner, M., Crewell, S., Ehrlich, A., Notholt, J., Lüpkes, C., Macke, A., Burrows, J. P., Rinke, A., Quaas, J., Maturilli, M., Schemann, V., Shupe, M. D., Akansu, E. F., Barrientos-Velasco, C., Bärfuss, K., Blechschmidt, A.-M., Block, K., Bougoudis, I., Bozem, H., Böckmann, C., Bracher, A., Bresson, H., Bretschneider, L., Buschmann, M., Chechin, D. G., Chylik, J., Dahlke, S., Deneke, H., Dethloff, K., Donth, T., Dorn, W., Dupuy, R., Ebell, K., Egerer, U., Engelmann, R., Eppers, O., Gerdes, R., Gierens, R., Gorodetskaya, I. V., Gottschalk, M., Griesche, H., Gryanik, V. M., Handorf, D., Harm-Altstädter, B., Hartmann, J., Hartmann, M., Heinold, B., Herber, A., Herrmann, H., Heygster, G., Höschel, I., Hofmann, Z., Hölemann, J., Hünerbein, A., Jafariserajehlou, S., Jäkel, E., Jacobi, C., Janout, M., Jansen, F., Jourdan, O., Jurányi, Z., Kalesse-Los, H., Kanzow, T., Käthner, R., Kliesch, L. L., Klingebiel, M., Knudsen, E. M., Kovács, T., Körtke, W., Krampe, D., Kretzschmar, J., Kreyling, D., Kulla, B., Kunkel, D., Lampert, A., Lauer, M., Lelli, L., von Lerber, A., Linke, O., Löhnert, U., Lonardi, M., Losa, S. N., Losch, M., Maahn, M., Mech, M., Mei, L., Mertes, S., Metzner, E., Mewes, D., Michaelis, J., Mioche, G., Moser, M., Nakoudi, K., Neggers, R., Neuber, R., Nomokonova, T., Oelker, J., Papakonstantinou-Presvelou, I., Pätzold, F., Pefanis, V., Pohl, C., van Pinxteren, M., Radovan, A., Rhein, M., Rex, M., Richter, A., Risse, N., Ritter, C., Rostosky, P., Rozanov, V. V., Donoso, E. R., Garfias, P. S., Salzmann, M., Schacht, J., Schäfer, M., Schneider, J., Schnierstein, N., Seifert, P., Seo, S., Siebert, H., Soppa, M. A., Spreen, G., Stachlewska, I. S., Stapf, J., Stratmann, F., Tegen, I., Viceto, C., Voigt, C., Vountas, M., Walbröl, A., Walter, M., Wehner, B., Wex, H., Willmes, S., Zanatta, M., and Zeppenfeld, S.: Atmospheric and Surface Processes, and Feedback Mechanisms Determining Arctic Amplification: A Review of First Results and Prospects of the (AC)3 Project, Bulletin of the American Meteorological Society, 104, E208 – E242, https://doi.org/10.1175/BAMS-D-21-0218.1, 2023.

Wendisch, M., Crewell, S., Ehrlich, A., Herber, A., Kirbus, B., Lüpkes, C., Mech, M., Abel, S. J., Akansu, E. F., Ament, F., Aubry, C., Becker, S., Borrmann, S., Bozem, H., Brückner, M., Clemen, H.-C., Dahlke, S., Dekoutsidis, G., Delanoë, J., De La Torre Castro, E., Dorff, H., Dupuy, R., Eppers, O., Ewald, F., George, G., Gorodetskaya, I. V., Grawe, S., Groß, S., Hartmann, J., Henning, S., Hirsch, L., Jäkel, E., Joppe, P., Jourdan, O., Jurányi, Z., Karalis, M., Kellermann, M., Klingebiel, M., Lonardi, M., Lucke, J., Luebke, A. E., Maahn, M., Maherndl, N., Maturilli, M., Mayer, B., Mayer, J., Mertes, S., Michaelis, J., Michalkov, M., Mioche, G., Moser, M., Müller, H., Neggers, R., Ori, D., Paul, D., Paulus, F. M., Pilz, C., Pithan, F., Pöhlker, M., Pörtge, V., Ringel, M., Risse, N., Roberts, G. C., Rosenburg, S., Röttenbacher, J., Rückert, J., Schäfer, M., Schaefer, J., Schemann, V., Schirmacher, I., Schmidt, J., Schmidt, S., Schneider, J., Schnitt, S., Schwarz, A., Siebert, H., Sodemann, H., Sperzel, T., Spreen, G., Stevens, B., Stratmann, F., Svensson, G., Tatzelt, C., Tuch, T., Vihma, T., Voigt, C., Volkmer, L., Walbröl, A., Weber, A., Wehner, B., Wetzel, B., Wirth, M., and Zinner, T.: Overview: quasi-Lagrangian observations

https://doi.org/10.5194/egusphere-2025-5831
Preprint. Discussion started: 28 November 2025

of Arctic air mass transformations – introduction and initial results of the HALO–$(\mathcal{AC})^3$ aircraft campaign, Atmospheric Chemistry and Physics, 24, 8865–8892, https://doi.org/10.5194/acp-24-8865-2024, 2024.

Wendisch, M., Kirbus, B., Ori, D., Shupe, M. D., Crewell, S., Sodemann, H., and Schemann, V.: Observed and modeled Arctic air-mass transformations during warm air intrusions and cold air outbreaks, Atmospheric Chemistry and Physics, 25, 15 047–15 076, https://doi.org/10.5194/acp-25-15047-2025, 2025.

Wesche, C., Steinhage, D., and Nixdorf, U.: Polar aircraft Polar5 and Polar6 operated by the Alfred Wegener Institute, Journal of large-scale research facilities, 2, A87, https://doi.org/http://dx.doi.org/10.17815/jlsrf-2-153, 2016.

Wu, P. and Ovchinnikov, M.: Cloud Morphology Evolution in Arctic Cold-Air Outbreak: Two Cases During COMBLE Period, Journal of Geophysical Research: Atmospheres, 127, e2021JD035 966, https://doi.org/10.1029/2021JD035966, e2021JD035966 2021JD035966, 2022.

Xia, Z. and McFarquhar, G. M.: Dependence of Cloud Macrophysical Properties and Phase Distributions on Environmental Conditions Over the North Atlantic and Southern Ocean: Results From COMBLE and MARCUS, Journal of Geophysical Research: Atmospheres, 129, e2023JD039 869, https://doi.org/10.1029/2023JD039869, e2023JD039869 2023JD039869, 2024.

Young, G., Jones, H. M., Choularton, T. W., Crosier, J., Bower, K. N., Gallagher, M. W., Davies, R. S., Renfrew, I. A., Elvidge, A. D., Darbyshire, E., Marenco, F., Brown, P. R. A., Ricketts, H. M. A., Connolly, P. J., Lloyd, G., Williams, P. I., Allan, J. D., Taylor, J. W., Liu, D., and Flynn, M. J.: Observed microphysical changes in Arctic mixed-phase clouds when transitioning from sea ice to open ocean, Atmospheric Chemistry and Physics, 16, 13 945–13 967, https://doi.org/10.5194/acp-16-13945-2016, 2016.